

UCSF

UC San Francisco Previously Published Works

Title

Alterations in corneal biomechanics underlie early stages of autoimmune-mediated dry eye disease

Permalink

<https://escholarship.org/uc/item/1cf6b49t>

Authors

Efraim, Yael

Chen, Feeling Yu Ting

Stashko, Connor

et al.

Publication Date

2020-11-01

DOI

10.1016/j.jaut.2020.102500

Peer reviewed

Alterations in corneal biomechanics underlie early stages of autoimmune-mediated dry eye disease

Yael Efraim^{1†}, Feeling Yu Ting Chen^{1†}, Connor Stashko², Ka Neng Cheong¹, Eliza Gaylord¹, Nancy McNamara^{3,4*} and Sarah M. Knox^{1*}

¹ Program in Craniofacial Biology, Department of Cell & Tissue Biology, University of California San Francisco, San Francisco, CA 94143, USA

² Center for Bioengineering and Tissue Regeneration, Department of Surgery, University of California San Francisco, San Francisco, CA 94143, USA

³ School of Optometry and Vision Science Graduate Program, University of California, Berkeley, CA 94720, USA

⁴ Department of Anatomy, University of California San Francisco, San Francisco, CA 94143, USA

†These authors contributed equally to this work.

* Authors to whom correspondence should be addressed: nmcnamara@berkeley.edu and sarah.knox@ucsf.edu.

Submission correspondence should be addressed to:

Sarah M. Knox

UCSF

513 Parnassus Ave HSE1510

San Francisco CA 94143

sarah.knox@ucsf.edu.

Abstract

Autoimmune-mediated dry eye disease is a pathological feature of multiple disorders including Sjögren's syndrome, lupus and rheumatoid arthritis that has a life-long, detrimental impact on vision and overall quality of life. Although late stage disease outcomes such as epithelial barrier dysfunction, reduced corneal innervation and chronic inflammation have been well characterized in both human patients and mouse models, there is little to no understanding of early pathological processes. Moreover, the mechanisms underlying the loss of cornea homeostasis and disease progression are unknown. Here, we utilize the autoimmune regulatory (*Aire*)-deficient mouse model of autoimmune-mediated dry eye disease in combination with genome wide transcriptomics, high-resolution imaging and atomic force microscopy to reveal a potential ECM-biomechanical-based mechanism driving cellular and morphological changes at early disease onset. Early disease in the *Aire-deficient* mouse model is associated with a mild reduction in tear production and moderate immune cell infiltration, allowing for interrogation of cellular, molecular and biomechanical changes largely independent of chronic inflammation. Using these tools, we demonstrate for the first time that the emergence of autoimmune-mediated dry eye disease is associated with an alteration in the biomechanical properties of the cornea. We reveal a dramatic disruption of the synthesis and organization of the extracellular matrix as well as degradation of the epithelial basement membrane during early disease. Notably, we provide evidence that the nerve supply to the cornea is severely reduced at early disease stages and that this is independent of basement membrane destruction or significant immune cell infiltration. Furthermore, diseased corneas display spatial heterogeneity in mechanical, structural and compositional changes, with the limbal compartment often exhibiting the opposite response compared to the central cornea. Despite these differences, however, epithelial hyperplasia is apparent in both compartments, possibly driven by increased activation of IL-1R1 and YAP signaling pathways. Thus, we reveal novel perturbations in corneal biomechanics, matrix organization and cell behavior during the early phase of dry eye that may underlie disease development and progression, presenting new potential targets for therapeutic intervention.

Keywords

cornea, limbal stem cells, biomechanics, dry eye disease, Sjögren's syndrome, sensory nerves, inflammation, extracellular matrix, basement membrane, barrier function, YAP, mechanosensor, autoimmune disease, autoimmunity.

Introduction

Aqueous-deficient dry eye is among the most common and debilitating clinical manifestations of systemic autoimmune diseases such as Sjögren's [1]. While it is well established that chronic inflammation of exocrine glands (e.g., lacrimal gland) represents the predominant driving force in autoimmune-mediated aqueous deficient dry eye disease [1], pathological alterations in the ocular surface are among the most common and debilitating clinical manifestations. With the ocular surface protecting the anterior eye from environmental, inflammatory and microbial insult, disease-mediated corruption of tissue function and homeostasis has a vast array of pathological outcomes. However, despite the known influence of inflammation on autoimmune-mediated dry eye, the timing of disease initiation and what drives early disease progression before immune cell infiltration remains unknown.

One of the ocular tissues most impacted by autoimmune-mediated dry eye disease is the cornea. The cornea is a non-vascularized transparent structure that provides approximately two-thirds of the eye's focusing power, and is the primary refracting component of the human visual system [2-4]. It also protects the anterior eye from environmental, inflammatory and microbial insult through an epithelial barrier composed of a multilayered epithelium (5-6 layers in mice, 8 in humans) that is separated from a highly organized collagen-rich stroma (also contains a sparse number of extracellular matrix-producing keratocytes) by an epithelial basement membrane (BM). The cornea is further compartmentalized spatially into the central and peripheral cornea and limbus, with the limbus providing KRT14+ stem cells that migrate centripetally to repopulate the organ under homeostatic conditions and in response to injury [5]. Changes at the ocular surface (e.g., pressure, temperature, pain) are sensed by nerves derived from the ophthalmic lobe of the trigeminal ganglia [6] that activate tear production from the lacrimal glands through the lacrimal reflex. Pathological changes to the ocular surface are also sensed by antigen presenting cells (undifferentiated dendritic cells) that reside throughout the stroma and epithelium to provide immune surveillance in an otherwise immune cell-deficient organ [7]. Autoimmune-mediated dry eye disease impacts each of these cellular components, with a multitude of studies in both human patients with Sjögren's and mouse models of aqueous deficient dry eye disease i.e., reduced tear fluid due to lacrimal gland dysfunction, illustrating late stage pathologies that encompass epithelial barrier disruption, epithelial hyperplasia, reduced corneal innervation and inflammatory cell infiltration [8-12]. However, no studies to date have revealed the timing of these changes during disease progression. As such, it is unclear, for example, if ocular surface inflammation precedes

epithelial barrier dysfunction or if epithelial barrier disruption precedes corneal denervation. Moreover, it is unknown if the signaling pathways known to be activated in late stage disease are also present early.

In addition to the known cellular changes induced in dry eye disease, recent studies in patients with Sjögren's using an ocular response analyzer (ORA) suggest that the biomechanics of the cornea are compromised in dry eye [13,14]. Biomechanical properties control the curvature of the cornea that is essential to light refraction and visual acuity [15], as well as cell behavior [16]. Corneal biomechanics are provided, by and large, by the composition and structure of the collagen-1-rich interstitial connective matrix of the stroma and the laminin-rich epithelial BM [17,18]. Ex vivo testing via atomic force microscopy (AFM) and Brillouin spectro-microscopy showed a gradient of stiffness across the healthy cornea, transitioning from a softer limbus to a stiffer central cornea. This gradient of stiffness is notably altered in diseases that impact the organization of collagen fibers in the stroma, as well as the packed collagen lamellae of Bowman's layer [19,20]. This is significant because alterations in stiffness have been shown to impact limbal stem cell behavior, with increasing stiffness promoting differentiation whereas softening induces cell proliferation and expansion [21]. Whether changes in the distribution of force occur across the cornea of patients with autoimmune-mediated dry eye is unknown.

To gain a better understanding of the early stages of autoimmune-mediated dry eye disease, we used a well-characterized, spontaneous mouse model of keratoconjunctivitis sicca combined with genome wide RNAsequencing, immunofluorescent validation and atomic force microscopy to conduct an unbiased exploration of early disease at the level of gene, protein expression and organ biomechanics. Mice deficient in autoimmune regulator gene (*Aire*) have a disruption in central tolerance that results in Th1 polarization of CD4+ T cells (secreting IFN γ)[22], an immune cell response that also occurs in patients with a variety of dry eye diseases including Sjögren's [23]. *Aire*-deficient mice exhibit classic signs of autoimmune-mediated exocrinopathy and associated aqueous-deficient dry eye over a matter of weeks, allowing for an interrogation of the molecular and cellular underpinnings of the disease in the absence of the effects of aging [24-26]. The disease progresses from small lymphocytic infiltrates in the lacrimal glands in 5 week (wk) old *Aire*^{-/-} mice, to extensive CD4⁺-T-cell-mediated exocrinopathy and expansion of B cell germinal centers, corneal pathologies, and severe dry eye by 7-8 weeks [10]. Here, we focus on alterations in the cornea during early disease progression to establish a cohort of phenotypic, genetic and biomechanical properties that correlate with early disease onset.

2. Materials and Methods

2.1 Animal Model

All procedures were approved by the UCSF Institutional Animal Care and Use Committee (IACUC) and were adherent to the NIH Guide for the Care and Use of Laboratory Animals (Approval number: 332AN089075-02). Wild type and *Aire*-deficient mice on the BALB/c background (BALB/c *Aire*^{-/-}) were the gift of Mark Anderson, University of California, San Francisco. Adult female mice (aged between 5 and 7 weeks) were used in all experiments. Mice were housed in the University of California San Francisco Parnassus campus Laboratory Animal Resource Center (LARC), which is AAALAC accredited. Mice were housed in groups of up to five per cage where possible, in individually ventilated cages (IVCs), with fresh water, regular cleaning, and environmental enrichment. Appropriate sample size was calculated using power calculations. Genomic DNA isolated from tail clippings was genotyped for the *Aire* mutations by PCR with the recommended specific primers and their optimized PCR protocols (Jackson Laboratories Protocol 17936).

2.2 Tissue processing and immunohistological analysis

Immunohistological and immunofluorescent analyses of cornea samples were performed as previously described [27]. Briefly, enucleated eyes were embedded in OCT Tissue Tek freezing media. 7µm and 20 µm sections were prepared from fresh frozen tissues using a cryostat (Leica, Izar, Germany) and mounted on SuperFrost Plus slides. Sections were fixed for 20 min in 4% paraformaldehyde (PFA) at room temperature (RT) and permeabilized using 0.3% Triton X100 in phosphate buffered saline for 15 min. Sections were then washed in PBST for 10 min, before being blocked with 5% normal donkey serum (Jackson Laboratories, ME) in PBST for 1 hour at RT. After blocking, slides were incubated with primary antibodies (diluted in blocking buffer) overnight at 4°C.

For chromogenic analysis, 7 µm tissue sections were treated with hydrogen peroxide for 15 min to quench the endogenous peroxidase activity prior to incubation with the primary antibody rat anti-CD4 (1:50, BD Pharmigen, Cat 550280). A Horseradish peroxidase conjugated secondary was used followed by amplification with DAB (Vector, SK-4100). Images were taken using Zeiss

Axio Imager 2 fluorescent microscope. The number of CD4+ T cells in the central corneal and limbal region was quantified by counting the absolute number of DAB+ brown cells with an associated nucleus labeled using H&E counterstain.

For immunofluorescent analysis, 7 or 20 μm tissue sections were incubated with the following primary antibodies: rabbit anti-TUBB3 (1:500, Cell Signaling, Cat 5568S), rat anti-Perlecan (HSPG) (1:500, Chemicon, MAB1948), goat anti-KRT12 (1:100, Santa Cruz, Cat 515882), rabbit anti-LAMA3 (1:500, Abcam, Cat 151715), rabbit anti-COL1 (1:500, Abcam, Cat 34710), rabbit anti-KRT4 (1:500, BioLegend, Cat 905301), rat anti-KRT19 (1:300, DSHB, Troma III), rabbit anti-YAP (1:100, Cell Signaling, Cat 4912S), rabbit anti-KLF4 (1:200, Abcam, Cat 214666), rabbit anti-pFAK (1:500, Abcam, Cat 223529), mouse anti-ZO1 conjugated to Alexa594 (1:1000, Life Technologies, Cat 339194), rat anti-Ecadherin (1:300, Life Technologies, Cat 131900), rat anti-K67 (1:100, Daiko, M7248), rabbit anti-POSTN (1:500, Abcam, Cat 14041). Antibodies were detected using Cy2-, Cy3- or Cy5-conjugated secondary Fab fragment antibodies (Jackson Laboratories), and nuclei were stained with Hoechst 33342 (1:3000, Sigma-Aldrich). Fluorescence was analyzed using a Zeiss Yokogawa Spinning disk confocal microscope with images assessed using NIH ImageJ software, as described below.

2.3 Image Analysis

Analysis of ECM and BM molecules and nerve density. Collagen type I (COL1) intensity was quantified in 300 μm sections of central cornea, or 200 μm sections of limbal stroma. Quantification was performed using a region of interest (ROI) and applying Tsai's thresholding method (Moments). Raw integrated densities normalized to the stromal area within the ROI of the thresholded image was recorded. COL1 images were also scored for fiber alignment, where corneal stroma with parallel fibers scored as 0, and complete misalignment scored as 5. Corneal stroma with score of 3 and above considered as misaligned (Supplementary Fig 2). Laminin (LAM) and perlecan (HSPG2) intensities were quantified on 300 μm sections of central cornea or 200 μm section of limbal epithelial basement membrane ROI applying Tsai's thresholding method (Moments) [28] or Yen's thresholding methods (Yen) [29], integrated densities within the ROI of the thresholded image were recorded. Periostin (POSTN) intensity was quantified on 200 μm sections of limbal stroma (ROI) and processed using Tsai's thresholding method (Moments).

Integrated densities were then recorded. Nerve density was quantified on 300µm sections of central cornea or 200µm sections of limbal epithelial ROI applying Tsai's thresholding method (Moments) or Yen, integrated densities within the ROI of the thresholded image were recorded.

Quantification of cell adhesion proteins and regulators. E-cadherin and ZO-1 fluorescent intensity was quantified in a region of interest (ROI) containing a 300 µm section of central cornea epithelium. A Tsai's thresholding method (Moments) was then applied to the ROI, and integrated densities within the ROI of the thresholded image were recorded. For KLF4, fluorescent intensity was quantified using Tsai's thresholding method (Moments) on basal cell nuclei (25 cells per cornea). Integrated density for each nucleus was recorded.

Quantification of mechanosensors pFAK and YAP. pFAK fluorescent intensity was quantified on a ROI containing a 300µm section of central cornea or a 200µm section of limbal epithelial basement membrane. Tsai's thresholding method (Moments) was applied to the ROI of each cornea, and integrated densities within the ROI of the thresholded image were recorded. The ratio of nuclear YAP to total cellular YAP was measured using Tsai's thresholding method (Moments) on basal cells (25 cells per central cornea, 15 cells per limbus). Integrated densities of total cellular YAP (marked by E-CAD) and nuclear YAP (marked by Hoechst) were recorded for each basal cell. Ratio of 1 equates to YAP being exclusively localized to the nucleus.

Quantification of basal cell proliferation. The number of KRT14+ cells and KRT14+Ki67+ cells were counted in the central cornea and limbal epithelium. To obtain the percentage of proliferating basal cells per respective region, cell counts were divided by the total number of KRT14+ cells.

Quantification of limbal cell expansion. Limbal epithelial progenitor cells were labeled using an antibody directed against KRT19. The ratio of KRT19 to cornea-specific KRT12 staining was calculated by measuring the relative length of tissue labeled with each marker when assessed limbus-to-limbus beginning at the KRT12 to KRT19 transition zone. The resulting ratio was used to quantitatively assess the extension of KRT19 into the cornea and, thus, expansion of the progenitor cells compartment. Epithelial thickness was measured at the central cornea and at the KRT12-KRT19 transition point. Basal cell height was measured on KRT14+ cells (25 cells per cornea).

Quantification of Epithelial Apoptosis. Apoptotic epithelial cells were labeled using an antibody directed against cleaved caspase 3 (CASP3). The number of CASP3+ epithelial cells was measured as a percentage of total ECAD+ epithelial cells within a 350µm region of the central cornea or 200µm region of the ECAD+ limbus.

2.3 Analysis of epithelial barrier function

Mice were anesthetized with isoflurane and 5 µL of lissamine green dye (1%) was applied to the lower conjunctival cul-de-sac. Images of the cornea were taken using an Olympus Zoom Stereo Microscope (Olympus, CenterValley, PA). Lissamine green staining was scored by dividing the cornea into four quadrants, the extent of staining in each quadrant was classified as Grade 0, no staining; Grade 1, sporadic (<25%); Grade 2, diffuse punctate (25-75%), or Grade 3, coalesced punctate staining (75% or more). The total score was calculated separately for each eye and equaled the sum of all four quadrants ranging from 0 (no staining) to 12 (most severe staining). Scoring was conducted by three masked observers with each data point representing the fold change relative to the average WT score from the same age group.

2.4 Tear Secretion Measurement

Mice were anesthetized with isoflurane and injected into the peritoneum (i.p.) with 4.5 mg/kg of pilocarpine diluted in saline. Ten minutes later, mice were anesthetized with isoflurane and tear secretion (as indicated by the length of the tear-absorbed region in 15 seconds) was measured using a Zone-Quick phenol red thread (Showa Yakuhin Kako Co. Ltd., Tokyo, Japan).

2.5 RNA isolation and RNAseq library generation

Total RNA was collected and purified using RNAaqueous and DNase reagents according to the manufacturer's instructions (Ambion, Houston, TX, USA). RNA quality was assessed using the Agilent 2100 BioAnalyzer, and samples with an RNA integrity number ≥ 6.0 were included for RNA sequencing. Up to 1 µg RNA was used to synthesize mRNA libraries using the TruSeq mRNA library kit (Illumina Inc, San Diego, CA, USA), as per the manufacturer's instructions.

2.6 RNAseq analysis

RNA libraries were sequenced on an Illumina HiSeq 4000. Depths of 20–30 million single-end 50 bp reads were generated for each sample. Quality control metrics were performed on raw sequencing reads using the FASTQC v0.11.6 application [30]. Reads were mapped to the UCSC *Mus musculus* genome mm10 (NCBI build v38) using Spliced Transcripts Alignment to a Reference (STAR) [31]. At least 90% of the reads were successfully mapped. Reads aligning to the mm10 build were quantified against Ensembl Transcripts release 93 using Partek® E/M (Partek's optimization of the expectation maximization algorithm, Partek Inc, St.Louis, MO, USA), which disregarded any reads that aligned to more than one location or more than one gene at a single location. Data was normalized by two procedures: 1. total count normalization, 2. addition of a small offset (0.0001). DEseq2 was then used to detect differential gene expression between WT and *Aire* *-/-* corneas based on the normalized count data. Genes were considered differentially expressed if the log₂ Fold Change between samples was at least 1, with the adjusted p-value held to 0.05 [32]. Volcano plot of differentially expressed genes were created using the “Enhancedvolcano” R package[33].

A list of all significantly modulated genes ($p < 0.05$) was used as input for gene ontology (GO) analysis and Kyoto Encyclopedia of Genes and Genomes (KEGG) pathway analysis using the online Database for Annotation, Visualization and Integrated Discovery (DAVID, version 6.8)[34]. We consider an attribute to be significant if its p value is less than 0.05 relative to an appropriate background gene set. The significantly differentiated gene list was also used as input for Gene Set Enrichment Analysis (GSEA) using GSEA software (Broad Institute- version 4.0.3) GSEA calculates normalized enrichment score that reflects overrepresentation of predefined genes sets in the *Aire* *-/-* compared to WT cornea control [35]

2.6 Atomic force microscopy (AFM)

Fresh intact corneas collected from 5 week *Aire* *-/-* and WT control mice were adhered to glass slides by PAP pen marking, allowing attachment for ~5 minutes. Corneas were then covered with media supplemented with 0.5% BSA to prevent protein deposition onto the cantilever. AFM measurements were obtained as described previously [36]. Briefly, AFM measurements were acquired using an MFP3D-BIO inverted optical AFM mounted on a Nikon TE2000-U inverted

fluorescent microscope (Asylum Research). Indentations were performed with silicon nitride cantilevers with a nominal spring constant of 0.06 N/m and borosilicate glass spherical tips 5 μm in diameter (Novascan Tech). Cantilever calibration was done using the thermal oscillation of the tip and via indentation of a thin mica sheet. Samples were indented at 2 $\mu\text{m/s}$ loading rate with a 1 V deflection voltage trigger. Force maps were obtained over eight points in 20x20 μm scan regions. Tissue stiffness (Elastic modulus) was computed using the Hertz model within the Asylum Research software with a sample Poisson Ratio of 0.5.

2.7 Statistical Analysis

A minimum of three independent repeats were conducted in all experiments. Bar graphs are used to summarize the means and standard deviations of each outcome obtained using all data collected from WT and *Aire*^{-/-} mice. A Student's t-test was used for two group comparisons, except for the elastic modulus comparison, where a Mann-Whitney U-test for non-normal distribution was used; $P < 0.05$ was considered statistically significant. A false discovery rate of 0.05 was applied to RNAseq data. A Wald test with Benjamini and Hochberg correction was used for differential gene expression, Fisher's exact test was used for GO and KEGG analysis, and Kolmogorov-Smirnov test was used for GSEA analysis.

3. Results

3.1 Early disease development in autoimmune-mediated dry eye disease is marked by a dramatic downregulation of basement membrane and extracellular matrix pathways

To identify key genes and pathways associated with the early stages of autoimmune-mediated dry eye disease, we profiled the transcriptomes of corneas from *Aire*^{-/-} and wild type (WT, i.e., *Aire*^{+/+}) mice at 5 weeks (wk) of age by RNA sequencing (RNAseq) and performed a differential gene expression analysis. Compared to the advanced disease state at 7 wk, which is characterized by severe dry eye with extensive lymphocytic infiltration of the lacrimal gland and cornea, as well as significantly reduced tear production [10], 5 wk *Aire*^{-/-} mice exhibited mild disease, with relatively low levels of CD4⁺ T cells infiltrating the lacrimal gland [27], central cornea, and limbus (Fig 1A,B), and a modest (~2-fold) reduction in stimulated tear secretion (Fig 1C). Using a false-discovery rate (FDR) cut-off of 0.05, we found extensive changes in gene expression between mutant and WT 5 wk corneas, with 931 genes upregulated (>2-fold; $p < 0.05$)

and 921 downregulated (>2-fold; $p < 0.05$, Fig 1D). Gene ontology (GO) and KEGG analyses of the RNAseq data set (Fig 1E and Supplementary Fig 1A,B) indicated significant enrichment of inflammatory signaling pathways that were also upregulated in 7 wk *Aire*^{-/-} mice [10], as well as other late stage SS mouse models [37]. Enriched pathways included cellular responses to interferon-beta (IFN β) and interferon-gamma (IFN- γ), antigen processing and presentation, and positive regulation of tumor necrosis factors (TNFs), T cell cytotoxicity, IL-1 β signaling and the JAK-STAT pathway (Fig 1E,F,1S). In contrast, pathways regulating epithelial cell behavior, including PI3K-AKT ($p=8.6 \times 10^{-9}$), Ras ($p=3.8 \times 10^{-3}$), and Wnt signaling ($p=1.2 \times 10^{-3}$; Fig 1E, F, S1B) were significantly downregulated. Strikingly, the greatest reduction in 5 wk *Aire*^{-/-} corneas belonged to the extracellular matrix (ECM; Fig 1E; 72 proteinaceous ECM genes, $p=1.7 \times 10^{-35}$), and sensory innervation (85 genes downregulated) with a significant depletion in pathways involved in collagen fibril organization ($p=1.1 \times 10^{-8}$), ECM-receptor interactions ($p=1.4 \times 10^{-11}$), synapses ($p=2.9 \times 10^{-9}$), and synaptic membranes ($p=9.8 \times 10^{-6}$).

To further delineate alterations in the ECM in the early stages of disease, we conducted Gene set enrichment analysis (GSEA) and validated our findings by immunofluorescent analysis. GSEA revealed a significant downregulation of mRNA encoding ~35% of the ~200 ECM-associated proteins in this gene set (Fig 2A), including transcripts coding for isoforms of the highly abundant stromal protein collagen I (COL1; *Col1a1* and *Col1a2* $p=2.43 \times 10^{-20}$ and $p=4.03 \times 10^{-38}$ respectively) and the BM protein laminin (*Lama1* and *Lama2* ($p=4.3 \times 10^{-4}$ and $p=1.51 \times 10^{-18}$ respectively; Fig 2B)). In addition, genes involved in ECM degradation, such as the metalloproteinases *Mmp9*, *10* and *13*, ($p=4.36 \times 10^{-6}$, $p=6.05 \times 10^{-6}$ and $p=1.05 \times 10^{-25}$, respectively) were upregulated (Fig 2B), further suggesting an alteration of ECM composition and structure at the earliest stages of disease development. Immunofluorescent analysis of the stromal ECM protein collagen 1 (COL1) and BM-enriched proteins heparan sulfate proteoglycan 2 (HSPG2/perlecan) and laminin alpha 3 chain (LAM, a component of the major corneal laminin, Laminin 332 [38]), confirmed structural disruption in these two compartments (Fig 2C-G). Although total levels of COL1 protein did not change in the *Aire*^{-/-} cornea (Fig 2C,D), more than 80% of the *Aire*^{-/-} mice showed a misalignment of collagen fibers in the corneal stroma (Supplementary Fig. 2), indicating severe disruption in ECM organization. Even more profound changes were observed in the BM, with significant depletion of both HSPG2 and LAM in the central cornea of 5 wk *Aire*^{-/-} compared to WT (Fig 2C,E,F,G). In conjunction with the reduction in the BM, KRT14+ basal cells changed from cuboidal to columnar, consistent with the known role of BM in regulating cell shape (Supplementary Fig. 3 [39]). Interestingly, these reductions were

limited to the central cornea, with the *Aire* ^{-/-} limbus exhibiting slightly increased levels of LAM and HSPG2 compared to the WT control (Fig 2E,F,G). Given this result, we further examined limbal ECM integrity using limbal-specific ECM protein periostin (POSTN) [40]. POSTN is known to play a role in the maintenance of limbal stem cells and is upregulated during wound healing [41]. We found increased POSTN protein in the *Aire* ^{-/-} limbal stroma compared to control (Fig 2H,I), suggesting an alteration in ECM composition in this region reflective of wound healing.

3.2 Disruption of the epithelial basement membrane and ECM are accompanied by corneal denervation in the early stages of dry eye development

ECM and BM components play an important role in growth and regeneration of the peripheral nervous system [42]. Consistent with the reduction in BM and ECM transcripts in the 5wk *Aire* ^{-/-} cornea, our differential gene expression analysis combined with GSEA revealed extensive downregulation of numerous neuronal genes and pathways associated with acetylcholine signaling (*Ache*, $p=4 \times 10^{-3}$, *Chrb1*, $p=3.8 \times 10^{-17}$), glutamate signaling (*Gria1*, $p=8.51 \times 10^{-27}$, *Gria2*, $p=3.5 \times 10^{-4}$), synapse formation (*Syp*, $p=3.7 \times 10^{-3}$, *Nrxn1*, $p=7.6 \times 10^{-6}$), axon guidance (*Ntn1*, $p=4.6 \times 10^{-4}$, *Slit3*, $p=2.7 \times 10^{-34}$, *Sema3c*, $p=2.35 \times 10^{-8}$) and nerve regeneration (*Gap43*, $p=1.1 \times 10^{-7}$) (Fig 3A). Immunofluorescent analysis of TUBB3⁺ corneal nerves validated these reductions, with a significant loss in nerve density throughout the cornea of 5 wk *Aire* ^{-/-} mice as compared to WT (Fig 3B-D). Surprisingly, despite the *Aire* ^{-/-} limbus showing similar or higher levels of BM proteins LAM and HSPG2 compared to the WT limbus, TUBB3⁺ fibers were significantly reduced throughout the ocular surface (Fig 3D), suggesting nerves are lost before the BM. Together, these data indicate that the corneal ECM and BM along with corneal innervation are significantly altered at the early stages of disease but that the BM and ECM of the limbal and central regions are differentially impacted.

3.3 Loss of epithelial junctions disrupts corneal epithelial barrier function

A key clinical indicator of dry eye disease severity in both humans and mice is a reduction in corneal epithelial barrier function [43]. This outcome is mainly due to a disruption in epithelial junctional complexes e.g., tight junctions, adherens junctions, and desmosomes, which are anchored to the intracellular cytoskeleton [44] to seal the paracellular space and provide structural support. We previously reported that 5 wk *Aire* ^{-/-} mice show very moderate corneal epithelial disruption compared to WT and late disease (7 wk *Aire* ^{-/-}) mice [27], indicating mild barrier dysfunction (Fig 4A). In support of these findings, our transcriptomic analysis revealed downregulation of genes associated with cell-cell junctions (Fig 4B), including junctional adhesion

molecules *Jam2* ($p=6.72 \times 10^{-24}$) and *Jam3* ($p=6.8 \times 10^{-7}$), tight junction associated marvel protein Claudin 10 (*Cldn10*, $p=8.09 \times 10^{-67}$), and type 1 transmembrane adhesion protein *Kirrel2/Neph3/filtrin* ($p=9 \times 10^{-5}$) [45] (Fig 4C). Alongside this reduction in epithelial junctional protein transcripts, we found a corresponding increase in the transcription of genes that serve to destabilize epithelial cell-cell adhesions such as Ephrin A2 (*Epha2*, $p=6.1 \times 10^{-14}$) [46], as well as genes involved in immune cell adhesion, including *Cd6* (*T cell adhesion receptor*, $p=1.8 \times 10^{-11}$), *Itgax/Cd11c* (*highly expressed by dendritic cells*, $p=2 \times 10^{-6}$), and *Itgal* (leukocyte intercellular adhesion, $p=5 \times 10^{-6}$; Fig 4C).

To further confirm the loss of epithelial barrier function in *Aire* $-/-$ corneas during early disease development, we examined expression patterns of proteins involved in the establishment and maintenance of barrier function. This included (i) Kruppel-like factor 4 (KLF4), a transcription factor highly expressed by corneal epithelial cells [47] that has been implicated in promoting corneal and epidermal cell differentiation [47] and barrier function [48,49]; (ii) the cell adhesion junction protein E-cadherin (ECAD), a critical mediator of epithelial cell-to-cell interactions [50]; and (iii) the tight junction protein zonula occludens-1 (ZO1), a key regulator of tight junction assembly [51] that is enriched in the apical squamous epithelial cells [52]. As shown in Figure 4D, KLF4 was expressed throughout the epithelial cell layers in WT corneas but was significantly reduced in the basal epithelial cells of 5 wk and 7 wk *Aire* $-/-$ mice (Fig 4D,G). Surprisingly, ECAD protein levels were dramatically elevated throughout the epithelium of 5 wk *Aire* $-/-$ corneas compared to WT before being significantly reduced at 7 wk (Fig 4E,H), suggesting that barrier dysfunction at 5 wk is not due to an early loss of ECAD-mediated cell-cell adhesions. We also found that total ZO1 expression levels in the *Aire* $-/-$ cornea were not significantly reduced at 5 wk or 7 wk compared to WT control (Fig 4F,I). However, expression of ZO1 by the apical cells was severely reduced, indicating a loss of barrier function (Fig 4F). This outcome mimics the pattern observed in wounded corneas deficient in syndecan-1 [53], suggesting the *Aire* $-/-$ cornea exhibits an early wound healing phenotype that is ultimately overridden by chronic inflammation.

3.4 Aberrant alteration in mechanical properties of the cornea influences cell behavior during the early stages of dry eye development

Alterations in ECM composition and organization have a profound impact on a tissue's mechanical properties, which in turn, influence cell behaviors including proliferation, migration, and differentiation [54-56]. Recent studies in the cornea have shown that epithelial cell proliferation and differentiation across the corneal surface is controlled by changes in stiffness,

with a softer substrate, promoting increased cell proliferation and reduced cell differentiation [40,57]. Given ECM deposition and organization heavily influences the mechanical properties of the corneal stroma [40], we hypothesized that breakdown of the BM along with disrupted organization of the stromal matrix of 5wk *Aire* *-/-* corneas would result in corneal softening. We employed atomic force microscopy (AFM) to evaluate the elastic properties of freshly isolated corneas with intact epithelia. For each cornea, three different fields, each consisting of eight distinct measurements (24 measurements in total), were obtained from both the central cornea and the limbal region. Compared to age-matched WT mice, we found the elastic modulus across the *Aire* *-/-* cornea to be significantly reduced within the central compartment but increased in the limbus (Fig 5A,B), supporting our hypothesis that the biomechanical properties of the tissue were altered early in disease.

Given this alteration in mechanical tension, we next asked whether activation of tissue mechanosensors were also altered in the 5 wk *Aire* *-/-* cornea. As shown in Figure 5, activation of focal adhesion kinase (FAK), a pivotal mediator of cell mechanosignaling that is phosphorylated (pFAK) when recruited to focal adhesions after integrin attachment to the ECM in a high-stiffness environment [58], was dramatically altered in the *Aire* *-/-* cornea. Compared to the WT cornea, where extensive pFAK accumulates at cell- to- matrix adhesion points along the BM, pFAK was markedly decreased in the central corneas of 5 wk *Aire* *-/-* mice where matrix softening was noted by AFM. In contrast, pFAK was notably increased within the limbal region where matrix stiffness was also increased (Fig 5C,D).

As pFAK has been shown to control the cytoplasmic to nuclear translocation, and thus activation, of the transcriptional co-activator Yes-associated protein (YAP) in response to mechanical stress [59,60], we next analyzed the expression pattern of YAP in WT and *Aire* *-/-* cornea. As shown in Figure 5, the central cornea exhibited similar YAP localization patterns in both WT and *Aire* *-/-* corneas, with the ratio of nuclear (active) to cytoplasmic (inactive) YAP highest in the basal epithelial cells. However, in contrast, we measured a significant increase in nuclear YAP in the limbal epithelial cells of the *Aire* *-/-* cornea compared to WT (Fig. 5E,F), supportive of increased YAP function in concordance with the increase in matrix stiffness measured by AFM.

Changes in tissue tension have been shown to strongly impact corneal stem cell behavior, with ECM stiffening promoting self-renewal and softening enhancing cell differentiation [57,61]. Based on these previous studies, we then asked whether limbal or central corneal stem/progenitor cells in 5 wk *Aire* *-/-* mice differed to WT in levels of cell proliferation or differentiation. Consistent with

the alteration in corneal biomechanics, we found early disease to be associated with an alteration in cell cycle entry. Using antibodies to the cell mitotic marker, Ki67, as well as the basal epithelial progenitor marker, keratin 14 (KRT14), we measured a significant increase in epithelial progenitor cell proliferation in both the limbus and central cornea of 5wk *Aire*^{-/-} cornea (Fig 5G,H), which resulted in tissue hyperplasia and corneal thickening (Fig. 5I). This outcome was complemented by a significant upregulation of *Krt14* gene expression (FC=4.5, $p= 3.95 \times 10^{-13}$; Fig. 1D). However, there was no increase in apoptotic (cleaved caspase-3+) epithelial cells in the *Aire*^{-/-} cornea at either 5 or 7 wk compared to wild type controls (Supplementary Fig. 4), suggesting alterations in the BM did not promote cell death. To define potential changes in progenitor cell expansion and differentiation, we examined expression of the epidermal marker KRT10 (not expressed in the healthy cornea epithelium) as well as measured the ratio of limbal KRT19+ to differentiated KRT12+ cells (KRT19/KRT12). Using these analyses, we previously showed ectopic expression of KRT10 by apical cells of the central cornea and expansion of limbal progenitor cells into the peripheral cornea from *Aire*^{-/-} mice at late stages of disease [10,62]. However, using the same approach, we failed to find expression of KRT10 protein and the limbal progenitor compartment had not yet expanded in 5 wk *Aire*^{-/-} mice, suggesting that corneal epithelial progenitors are yet to undergo aberrant epidermal transformation and that the stem cells remain within the limbal niche during the early stages of disease development (Fig 5J,K).

Discussion:

In this study we reveal the molecular, cellular, mechanical and compositional alterations that take place in the murine cornea during early stages of autoimmune-mediated dry eye disease. We demonstrate for the first time that early disruptions in ECM and BM synthesis and organization occur during the emergence of autoimmune-mediated dry eye disease and are associated with alterations in the cornea's mechanical properties. We also show that corneal barrier function, cellular homeostasis and sensory innervation are detrimentally impacted at the early stages of disease development, well before significant immune cell infiltration of the cornea. Further, we find that the profound loss of corneal nerves occurs independent of changes in BM deposition, suggesting that desiccating stress alone is sufficient to promote denervation. Finally, we newly demonstrate that the early diseased cornea displays spatial heterogeneity in the majority of these mechanical, structural and compositional changes, with the limbal compartment often exhibiting the opposite response compared to the central cornea. Thus, we reveal novel perturbations in corneal biomechanics, matrix organization and cell behavior during the early phase of dry eye

that may underlie disease development and progression, presenting new potential targets for therapeutic intervention.

A key outcome from our study was the discovery of altered corneal biomechanics at the early stages of dry eye disease. A number of studies have shown changes in biomechanical properties are associated with corneal pathologies [63]. Ocular response analyzer (ORA) and Corneal Visualization Scheimpflug Technology (CorVis ST) measurements in patients with Sjögren's at late stages of disease have previously suggested that the biomechanics of the cornea are compromised in dry eye [13,14]. These studies show the cornea of Sjögren's patients to have reduced stiffness as compared to healthy controls but when this outcome occurs and what induces these changes are unknown. Our data suggests that altered corneal stiffness is likely the result of altered ECM and/or BM composition and organization. The biomechanics of the cornea, like all tissues, are tied to the structure and composition of the ECM. ECM stiffness is determined by the amount of proteins present, such as collagens, fibronectin or proteoglycans, their spatial orientation and organization, their degree of crosslinking, and their regulation/remodeling by matrix metalloproteinases [64]. Thus, it is not surprising that the extensive reduction in global ECM gene expression and heightened production of MMPs in the *Aire* ^{-/-} cornea during early disease would be strongly associated with significant alterations in the elastic modulus of the tissue. Whether this is also the case in humans remains to be investigated.

Essential to visual acuity is the curvature of the cornea, which is achieved, in part, through spatial heterogeneity of tissue tension. Measurements of healthy human and murine cornea biomechanics using nonlinear optical (NLO) imaging techniques along with AFM and Brillouin spectro-microscopy (BSM) identified critical biomechanical differences between the limbus and the central cornea needed for tissue homeostasis and visual acuity [40,57,65,66]. That is, substrate stiffness increases from the limbus to the central cornea. In mice, the soft limbal region has been shown to be required for maintaining the stem cell niche and increasing centripetal stiffness that is essential for driving progenitor cell differentiation [40,57]. In our study, we unexpectedly found that changes in stiffness during early disease were region specific and were in opposition to the existing forces i.e., we found central cornea softening and limbal stiffening. In vivo ORA/CorVis ST measurements of human cornea with late stage dry eye disease reveal cornea softening [13,14], however, as these techniques do not allow regional analysis, the impact on central vs. peripheral tissue is unclear. In line with previous murine studies showing that corneal softness drives cell proliferation and disables differentiation [67-69], we found increased

KRT14+ progenitor cell proliferation in the central cornea, as well as a reduction in basal expression of the pro-differentiation factor KLF4, suggestive of an early impairment in cell differentiation. Indeed, impaired KRT14+ cell differentiation is found in the 7 wk *Aire*^{-/-} cornea [10]. However, despite the 5wk *Aire*^{-/-} cornea showing elevated limbal stiffness and increased nuclear YAP, which we predicted based on other studies would provoke differentiation and reduce proliferation [40,57], limbal epithelial cell proliferation increased. Moreover, YAP remained active in the softening central cornea even in the absence of its activator pFAK. These outcomes suggest that YAP localization and function during the earliest stages of dry eye development differs from that of the healthy cornea. In support of this, YAP has been shown to be activated and translocated to the nucleus in intestinal epithelial cells in response to inflammatory signals so as to promote epithelial cell proliferation and regeneration [70]. Whether YAP is indeed activated by inflammatory factors produced by the corneal epithelium to promote epithelial proliferation remains to be investigated.

In addition to contributing to tissue biomechanics, the epithelial BM and stromal ECM have a multitude of critical cellular functions. The BM is needed for anchoring epithelial cells, modulating cell migration and differentiation, and maintaining the differentiated phenotype of associated epithelial cells [71], while production of proteoglycans (e.g., lumican) and growth factors/cytokines by keratocytes in the stroma contributes to wound healing [72,73]. Thus, not surprisingly, alterations to the corneal BM and stromal ECM have been described in multiple human corneal pathologies including keratoconjunctivitis sicca [74], corneal epithelial basement membrane dystrophy [75], and diabetic keratopathy [76]. Each of these disorders can severely impact epithelial barrier function, wound repair, and/or cell identity. However, as studies to date have solely focused on late stage disease, it is unknown whether disruption in the BM and ECM occurs early or late during disease development.

Our findings showing extensive ECM disruption and remodeling at early disease stages suggest that clinical characteristics of dry eye disease, believed to be driven by inflammation, may be mediated through an increase in matrix degradation and a reduction in ECM synthesis. Two recent studies using mouse models of non-autoimmune-mediated dry eye attribute disorganization of the stromal ECM and loss of the BM to tissue remodeling by matrix metalloproteinases produced by the corneal epithelial cells in response to desiccating and osmotic stress [77,78]. Consistent with these studies, we found increased transcript levels of epithelial *Mmp9*, which has been shown to impair epithelial cell adhesion by cleaving laminin,

collagen IV and beta4 integrin [79,80], and MMP13, which degrades perlecan/HSPG2 [81], at the early stage of disease. Increased production of MMPs, including MMP-9, have been measured in the tears of patients with aqueous deficient dry eye disease [82,83], although whether this impacts the ECM or BM has not been determined. Furthermore, whether MMPs are elevated in the stroma of patients with dry eye disease or if BM and ECM synthesis are also reduced, as for the *Aire*^{-/-} model, is unknown. However, with changes in MMP levels in the *Aire*^{-/-} cornea being relatively small compared to the dramatic reduction in global ECM gene expression, our data strongly suggests that a loss of ECM synthesis by corneal epithelial cells and stromal keratocytes contributes significantly to alterations in both the BM and stromal ECM and thus tissue tension. What cellular events or signaling pathways mediate these transcriptional changes in ECM and MMP genes remains unclear. However, it is known that epithelial MMP gene expression is activated by stress-associated mitogen-activated protein kinase signaling pathways (including c-Jun N-terminal kinase, extracellular signal-related kinase, and p38) downstream of proinflammatory cytokines (e.g., IL-1b, TNFs, and IL-6) and upstream of transcription factors nuclear factor κB and activator protein 1 [84-88], all of which are elevated in the 5 wk *Aire*^{-/-} cornea. Similarly, immune factors such as IL-1 modulate the production of collagenases, metalloproteinases, and other enzymes by keratocytes [89]. Thus, we predict these pathways are also involved in altering ECM and MMP gene expression in autoimmune-mediated dry eye.

This significant loss of ECM and BM in the early stages of dry eye development raised some compelling questions regarding the molecular events that link altered biomechanics with disease pathogenesis. Loss of ECM and BM closely paralleled compartment-specific softening of the central cornea suggesting that quantitative assessment of the cornea's biomechanical behavior could offer a viable modality to diagnose, monitor, and manage dry eye disease during its earliest stages, even before the onset of chronic inflammation and extensive tissue damage. The prospective clinical application of corneal biomechanics in the setting of disease diagnosis and management is currently under investigation to assess the risk of ectasia in corneal disorders, such as keratoconus and following refractive surgery [90]. As such, there has been considerable interest in developing novel technologies like the Ocular Response Analyzer (Reichert Ophthalmics) that can provide point-of-care assessment of corneal biomechanical responses [91].

Structural integrity of the corneal basement membrane and underlying stroma is critical to maintain homeostasis and to support the viability of its extensive network of sensory nerves. A

functional nerve supply is essential to corneal homeostasis, as well as the production of tears, through activation of the lacrimal reflex. Dry eye disease in humans is heavily associated with altered innervation [92], yet the time point at which the nerve supply is reduced during disease progression and the identity of the factors driving denervation are unknown. We recently reported that 7wk *Aire*^{-/-} corneas exhibit a profound reduction in sensory innervation and tear secretion that occurred in conjunction with extensive immune cell infiltration [10]. Our current study indicates that denervation occurs very early in disease development and likely precedes immune cell infiltration of the cornea. Furthermore, similar to the global corneal denervation exhibited at late stage disease, we also found a dramatic reduction in the nerve supply to both the limbus and central cornea at the early disease timepoint. Intriguingly, however, loss of innervation to the 5 wk *Aire*^{-/-} limbus occurred despite the presence of LAM-enriched BM, which has been well described as a prerequisite for axon development and regeneration [93,94]. Such an outcome predicts that other factors important for nerve maintenance are being lost. In support of this notion, we measured significant reductions in expression of genes that participate in axon guidance, including *Ntng1*, *Slit1-3* and *Sema3c*. Notably, a recent study investigating the role of SEMA3C in the wounded corneas of wild type and diabetic mice (these mice also display reduced corneal innervation) showed that SEMA3C levels are greatly elevated in the epithelium of healthy but not diabetic mice, and that in vivo addition of exogenous SEMA3C to the diabetic mouse cornea improved sensory nerve regeneration [95].

A hallmark of dry eye disease is epithelial barrier disruption that enables pathogens, allergens and irritants to enter the eye. This phenotype largely results from a loss in functional cell-cell adhesion complexes such as tight junctions and cadherin-catenin complexes, or a reduction in epithelial cell adhesion to the BM. We found that each of these junctional interactions were disrupted at late stage disease (7 wk), with a severe loss of ZO1 in the apical corneal epithelial cells, reduced E-cadherin expression and the absence of BM proteins. However, despite increased epithelial barrier dysfunction in the 5wk *Aire*^{-/-} cornea compared to WT, at the early disease time point ZO1 was still expressed by suprabasal cells while Ecadherin became highly enriched throughout the epithelium. Such an upregulation in Ecadherin expression has previously been observed in other autoimmune disorders including inflammatory bowel disease, where acute inflammation was associated with upregulated Ecadherin whereas chronic inflammation reduced cadherin complexes [96]. A possible mechanism underlying epithelial barrier dysfunction at the early disease stage is increased expression of proinflammatory cytokines by the corneal epithelium. TNF- α , IFN- γ and IL-1 β are expressed by multiple epithelial organs, including the 5wk

Aire^{-/-} cornea, in response to stress or damage and serve in the initiation and amplification of the inflammatory response [97]. In addition, each of these cytokines has been shown to disrupt the barrier function of a variety of epithelial cells, including retinal pigment and intestinal epithelial cells [98,99]. Notably, exogenous treatment of human corneal epithelial cells with IL-1 β demonstrated a loss of apical ZO1 in a time dependent manner [100]. Together, these studies suggest that the epithelium attempts to preserve its barrier function in acute disease but that, over time, chronic inflammation reverses this outcome.

In addition to being a regulator of barrier function in multiple epithelial tissues, IL1/IL1R signaling is also a key modulator of corneal inflammation and wound healing, where it is activated in response to desiccating stress or acute injury. IL-1 serves to regulate many of the most important responses to corneal injury, including mobilization of inflammatory cells and up-regulation of the production of molecules involved in the defense against pathogens, angiogenesis, stromal remodeling, and the elimination of wound healing cells [89]. Previously, we demonstrated a central role for the IL-1/IL-1R cytokine signaling pathway in the *Aire*^{-/-} mouse model of dry eye [101], where it served as an essential mediator of epithelial hyperplasia and CD4⁺ T cell-mediated inflammation. In accordance with these studies, we found an upregulation of IL-1 β mRNA (FC=8.5, $p=2.53 \times 10^{-12}$), and transcripts involved in both the production and cellular response to IL-1, as well as hyperproliferative epithelial cells throughout the cornea. However, this was in the near absence of adaptive immune cell invasion. Moreover, there was an enrichment of gene set profiles associated with acute wound healing. These included innate defense processes such as the release of proinflammatory cytokines by ocular epithelial cells (e.g., IL-1 β , TNFs, IL-6), antigen presentation and processing, and activation of stress-induced signaling pathways. Persistent activation of these pathways will promote disease progression and result in chronic inflammation. Thus, these results suggest that the earliest stages of dry eye disease development resemble the innate stress response of wound healing, as opposed to the chronic inflammatory phenotype of late disease, and are driven, in part, by IL1 signaling [102].

In summary, our data demonstrate the novel and compelling impact of altered tissue biomechanics on cell behavior and early disease development in a mouse model of spontaneous, autoimmune-mediated, aqueous-deficient dry eye. Changes in cell behavior occur in conjunction with ECM-based softening of the cornea, which we postulate to be essential to disease development and progression. Intriguingly, changes in corneal biomechanics and cell behavior

are initiated prior to the extensive infiltration of CD4⁺ T-cells, indicating that these changes are associated with an early wound healing response as opposed to chronic inflammation.

Moving forward, it will be important to closely examine the molecular events that disrupt the corneal basement membrane during dry eye development and its impact on cell behavior (e.g., cell-cell adhesion, proliferation, and differentiation), tissue biomechanics, sensory innervation, and inflammation. A more thorough understanding of the sequence of events that leads to chronic dry eye and the interactions between associated pathways is paramount to identifying novel therapeutic approaches that break the cycle of disease development at its earliest stages.

Acknowledgements

The authors would like to thank Aaron Sullivan, Dylan Huynh and Matthew Koppinger for their contribution to the research, and Danit Efraim for the AFM illustration. Funding: This work was supported by the National Eye Institute (NEI; R01EY025980; R01EY026492; R01EY027392) and the National Institute of Dental and Craniofacial Research (NIDCR; 1R35DE028255). This work was made possible, in part, by NEI P30 EY002162 - Core Grant for Vision Research.

Author contributions

Y.E, F.Y.C., S.M.K and N.A.M. designed experiments and wrote the manuscript. Y.E., F.Y.C., C.S., K.N.C., and E.A.G. performed experiments. F.Y.C performed the RNA isolation and RNAseq library preparation. Y.E. performed the bioinformatics analysis of the RNAseq data and Y.E. and S.M.K interpreted the data. C.S. and Y.E. performed AFM measurements and analysis. Y.E., and F.Y.C. performed imaging and data analysis. S.M.K. and N.A.M. directed the project. All authors have read and agreed on the manuscript.

Figure Legends

Figure 1: Dramatic downregulation of pathways associated with basement membrane/extracellular matrix synthesis and functional innervation during early disease occurs in conjunction with the enrichment of inflammatory pathways that regulate corneal wound healing. (A) Immunohistochemical analysis and (B) quantification of CD4⁺ T cells in the central cornea (cCo) and limbus (Lm) of 5 wk WT and *Aire*^{-/-} mice. (C) Pilocarpine-induced tear secretion of 5 wk WT and *Aire*^{-/-}. (D) Volcano plot shows the number and magnitude of

differentially expressed genes in the 5 wk *Aire* ^{-/-} vs. WT cornea. The plot indicates -log₁₀ p-value for genome-wide genes (Y-axis) plotted against their respective log₂ fold change (X-axis). The red and blue dots represent significantly up- and down-regulated genes (fold change > 2, p-value < 0.05), respectively. (E) Heat map of representative genes associated with immune response, PI3K-AKT signaling, cell differentiation, Ras, and Wnt signaling. (F) Ranked list of biological pathways (gene ontology (GO) analysis) that are enriched during early disease. Scale bar = 50 μM. * p < 0.05; ** p < 0.01; *** p < 0.001, unpaired two-tailed t-test. Each dot in the bar graph represents a biological replicate. Error bars represent standard deviation.

Figure 2: The composition and structure of the extracellular matrix and basement membrane are disrupted and exhibit spatial heterogeneity during early disease. (A) Enrichment score (ES) from GSEA analysis demonstrates significant downregulation of genes associated with corneal extracellular matrix in 5 wk *Aire* ^{-/-} vs WT corneas. (B) Corresponding heatmap highlighting the relative expression of the extracellular matrix gene set. (C) Immunofluorescent analysis of whole cornea for collagen I (COL1) and perlecan (HSPG2) in 5 wk WT and *Aire* ^{-/-} corneas. Sets outlined in yellow and red show magnified images of the central cornea (cCo) and limbus (Lm), respectively. (D) Quantification of COL1 fiber density in the corneal and limbal stroma of WT and *Aire* ^{-/-}. (E) Quantification of HSPG2 in the basement membrane of the central cornea and limbus. (F and H) Immunofluorescent analysis (G and I) and quantification of basement membrane markers laminin alpha 3 (LAM, central cornea and limbus) and limbal-specific ECM marker, periostin (POSTN), in the limbus of 5 wk WT and *Aire* ^{-/-} corneas. Scale bar = 25 μM for F and G as well as inset small images in C, and 200 μM for whole cornea in C. * p < 0.05; ** p < 0.01; unpaired two tailed t test. Each dot in the bar graph represents a biological replicate. Error bar represents standard deviation.

Figure 3: Loss of central cornea innervation at early disease. (A) Heatmap highlighting relative expression of neuronal genes associated with acetylcholine signaling, glutamate signaling, synapses formation, nerve regeneration, and axon guidance pathways. (B) Cornea from 5 wk WT and *Aire* ^{-/-} were immunostained for the pan-neuronal marker beta3 tubulin (TUBB3) and corneal epithelial marker keratin 12 (KRT12). The image of the whole peripheral+central cornea was generated through a tiling function using 1 μm confocal sections, with yellow and red outlined insets showing magnifications of the central cornea (cCo) and limbus (Lm). Epithelial marker E-cadherin (ECAD) was shown together with TUBB3 in the limbus. (C-D) Quantification of TUBB3 nerve density in central corneal and limbal epithelium. Scale bars in B

are 25 μM for inset images and 200 μM for intact cornea. * $p < 0.05$; ** $p < 0.01$; unpaired two tailed t test. Each dot in the bar graph represents a biological replicate. Error bars represent standard deviation.

Figure 4: Loss of apical tight junctions and their regulators in early disease. (A) Lissamine green staining indicates the extent of ocular surface epithelial damage in health, early disease (5wk) and late disease (7wk) *Aire*^{-/-} mouse. (B) GSEA analysis of *Aire*^{-/-} vs WT cornea revealed a reduction in genes associated with cell adhesion. A plot of the Enrichment Score (ES) vs. the gene list index is shown in B. (C) Corresponding heatmap highlighting the relative expression of the genes belonging to the cell adhesion gene set. (D-I) Immunofluorescent analysis (D-F) and quantification (G-I) of the transcription factor KLF4 (D and G), the cell-cell adhesion molecule ECAD (E and H), and the tight junction protein ZO1 (F and I) in healthy, early disease (5wk) and late disease (7wk) cornea. The graph in G shows expression levels of KLF4 in the basal epithelial cells. Graphs in H and I show expression levels of ECAD and ZO1 throughout the epithelium. Scale bar = 25 μM . * $p < 0.05$; ** $p < 0.01$; *** $p < 0.001$; unpaired two tailed t-test. Each dot in the bar graph represents a biological replicate. Error bars represent standard deviation. Each dot in the box plot represents a cell. $n > 4$ mice per group.

Figure 5: Softening of the central cornea and aberrant activation of mechanotransduction at the limbus during early disease. (A) Schematic depiction of atomic force (AFM) microscopy experimental design in fresh whole mount corneas from 5wk WT and *Aire*^{-/-} ($n = 3$ per group). Three force maps of eight measurements each per central cornea and limbus were taken. (B) Elastic modulus of the central cornea and limbus derived from AFM force maps in 5 wk WT and *Aire*^{-/-}. Each dot in the bar graph represents a measurement within a force map. (C-F) Immunofluorescent analysis and quantification for the tissue mechanosensors pFAK (C and D) and YAP (E and F). For pFAK, fluorescence levels at the epithelial-BM border were measured (D). For YAP (F), quantification is represented by a heatmap for the ratio of nuclear YAP to total YAP protein expressed in basal epithelial cells with each horizontal line in each column representing a cell. (G and H) Immunofluorescent analysis and quantification of basal progenitor cell proliferation using the cell cycle marker Ki67 and progenitor cell marker KRT14 in cCo and Lm epithelium of 5 wk WT and *Aire*^{-/-}. The dotted white line outlined the limbal epithelium. (I) Quantification of epithelial thickness in central cornea and limbus of 5wk WT and *Aire*^{-/-}. (J and K) Immunofluorescent analysis of KRT19 (marks limbal epithelial cells) and KRT12 (specific to peripheral/central cornea epithelial cells) in the 5 wk WT and *Aire*^{-/-} cornea. (K) Quantification

for expansion of limbal progenitors indicated by KRT19 to KRT12 ratio. Scale bar = 25 μ M. * $p < 0.05$; ** $p < 0.01$; *** $p < 0.001$; unpaired two tailed t test except for B where a Mann-Whitney test was applied. Each dot in the bar graph represents a biological replicate. Error bars represent standard deviation.

Figure 1

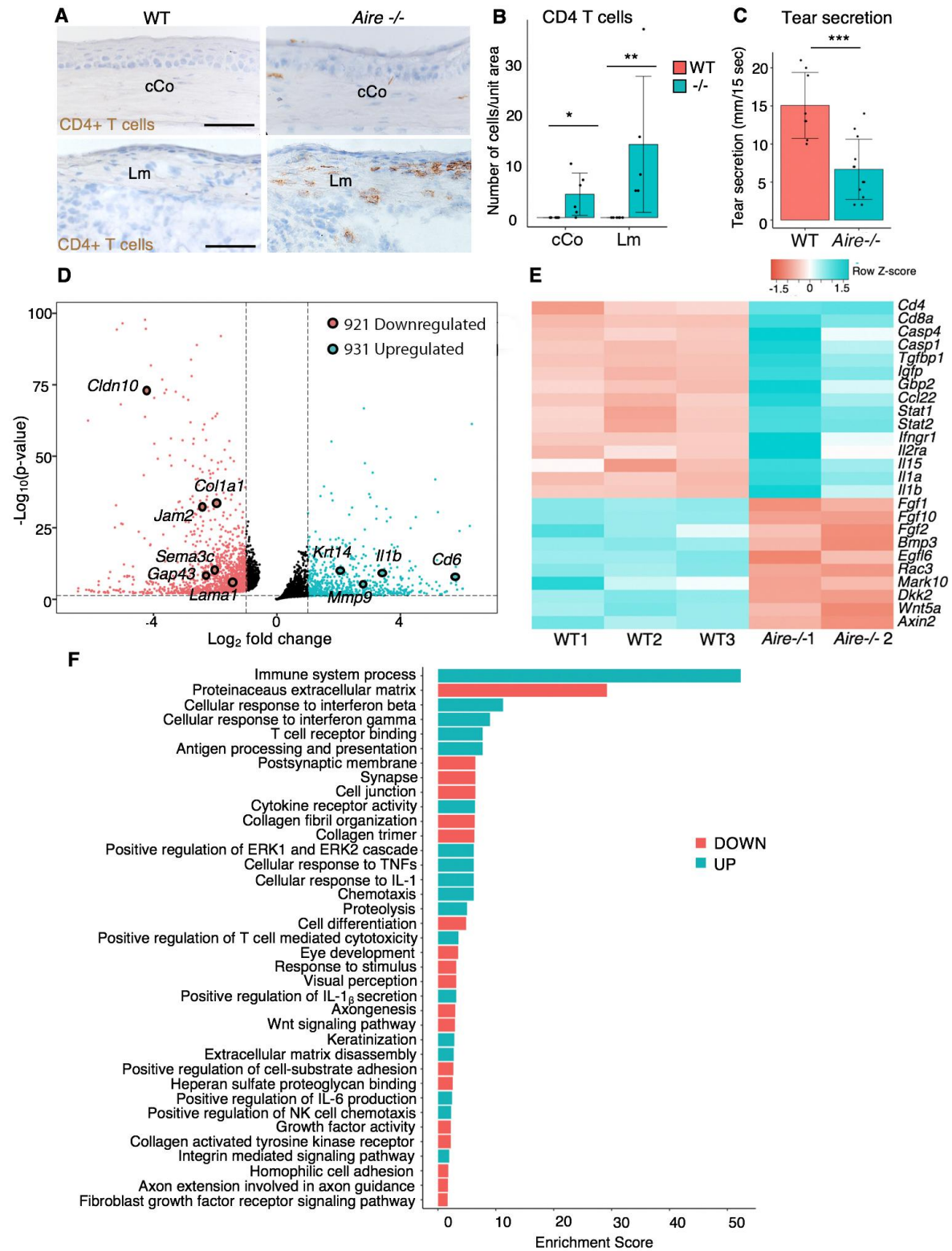


Figure 2

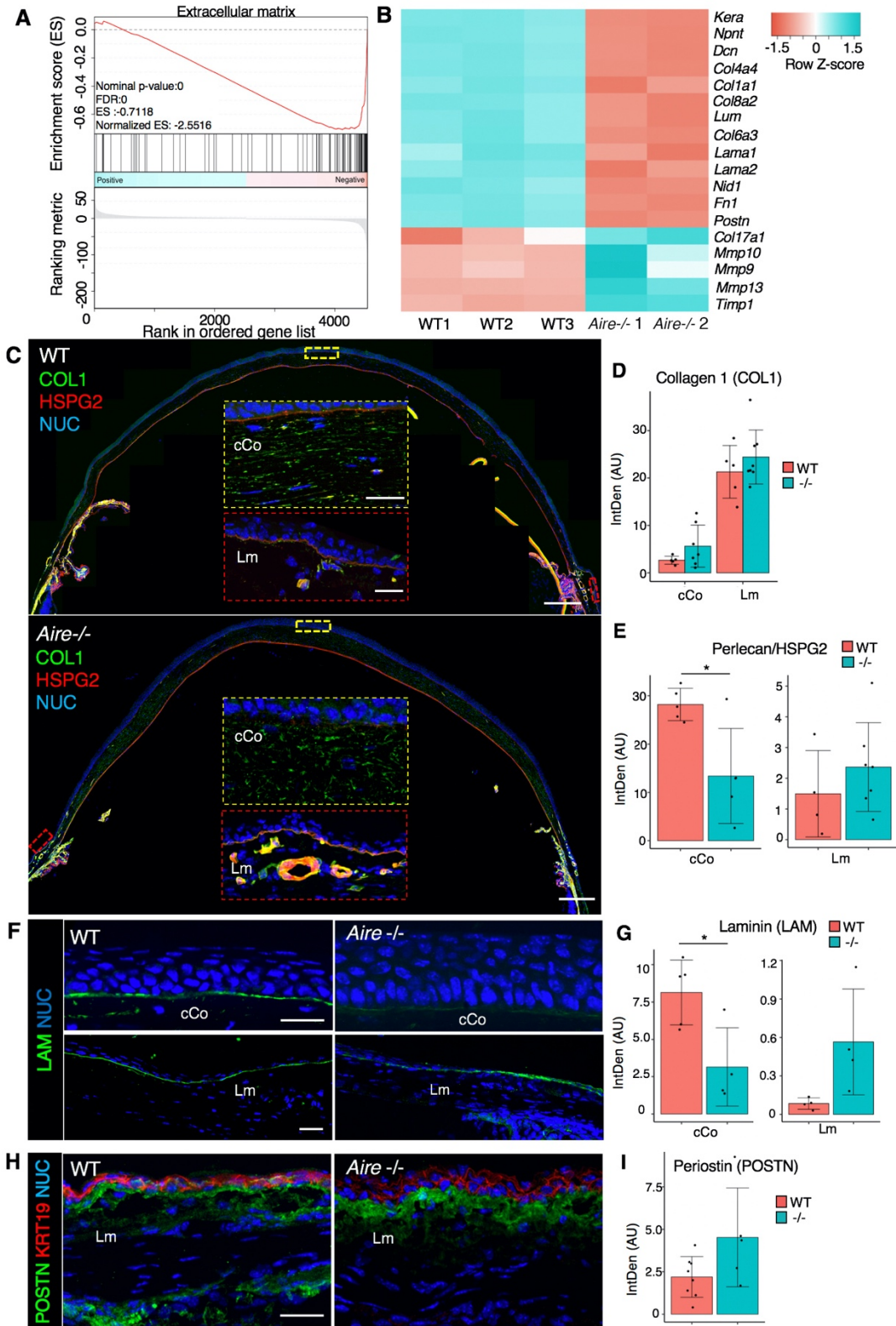


Figure 3

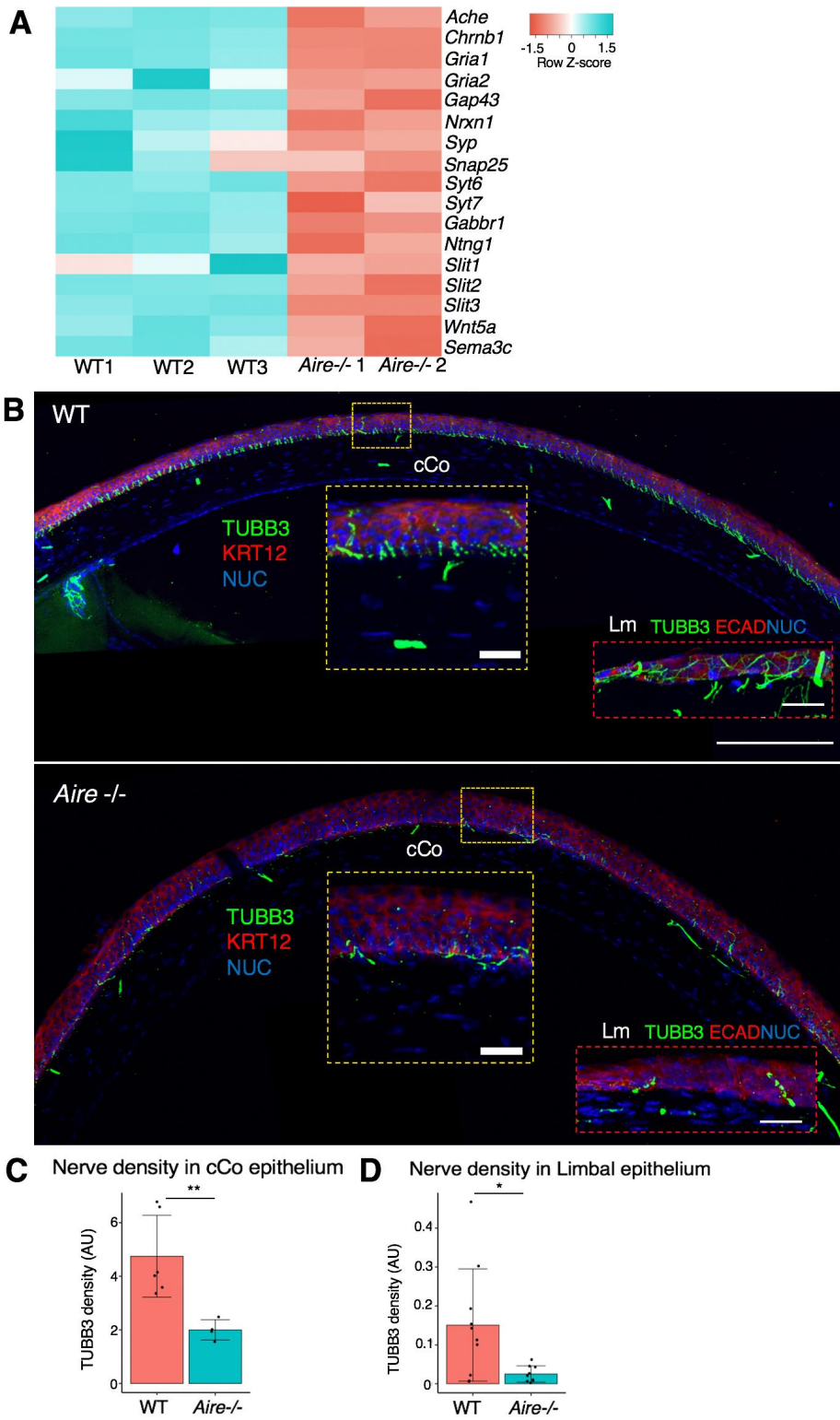


Figure 4

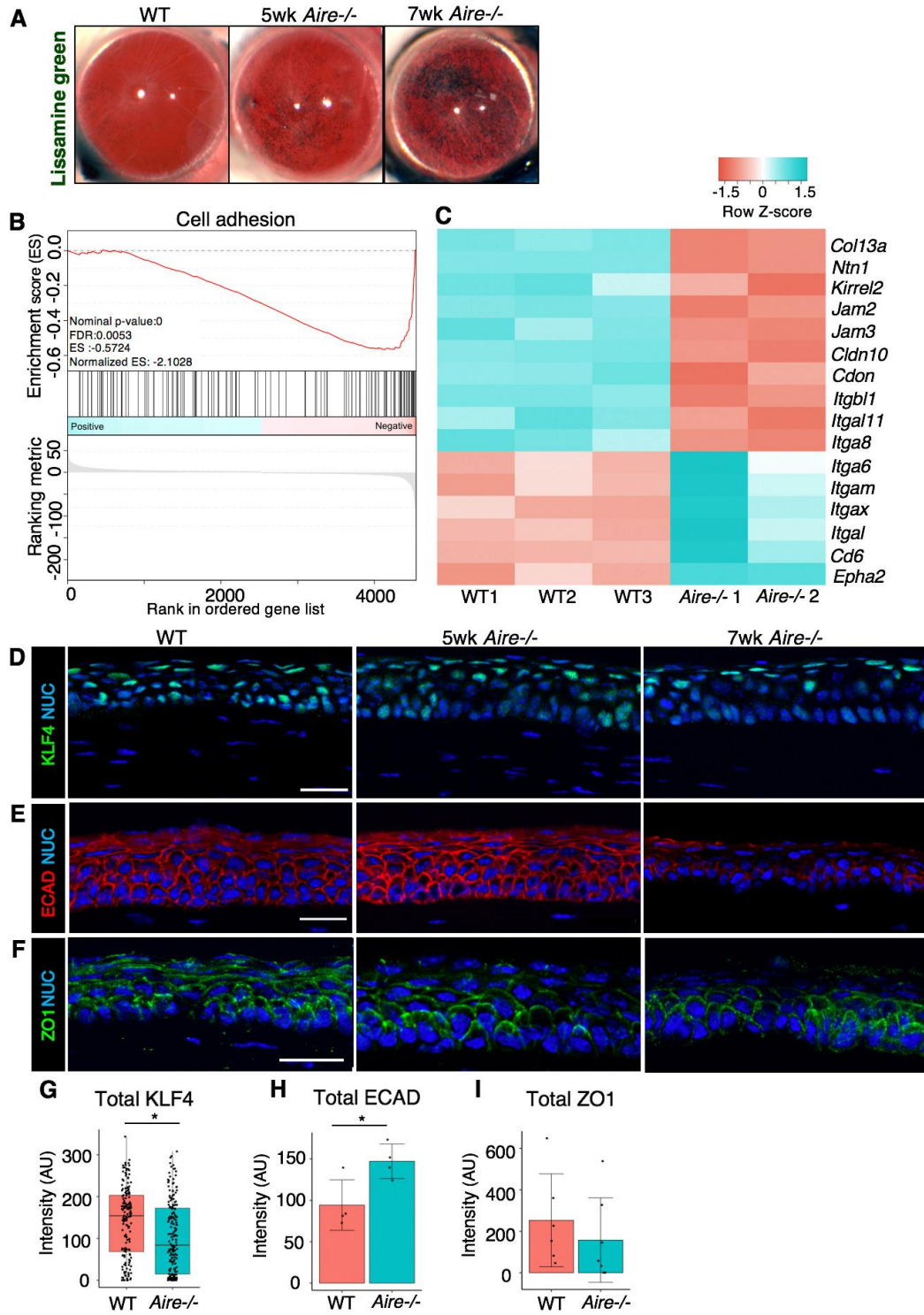
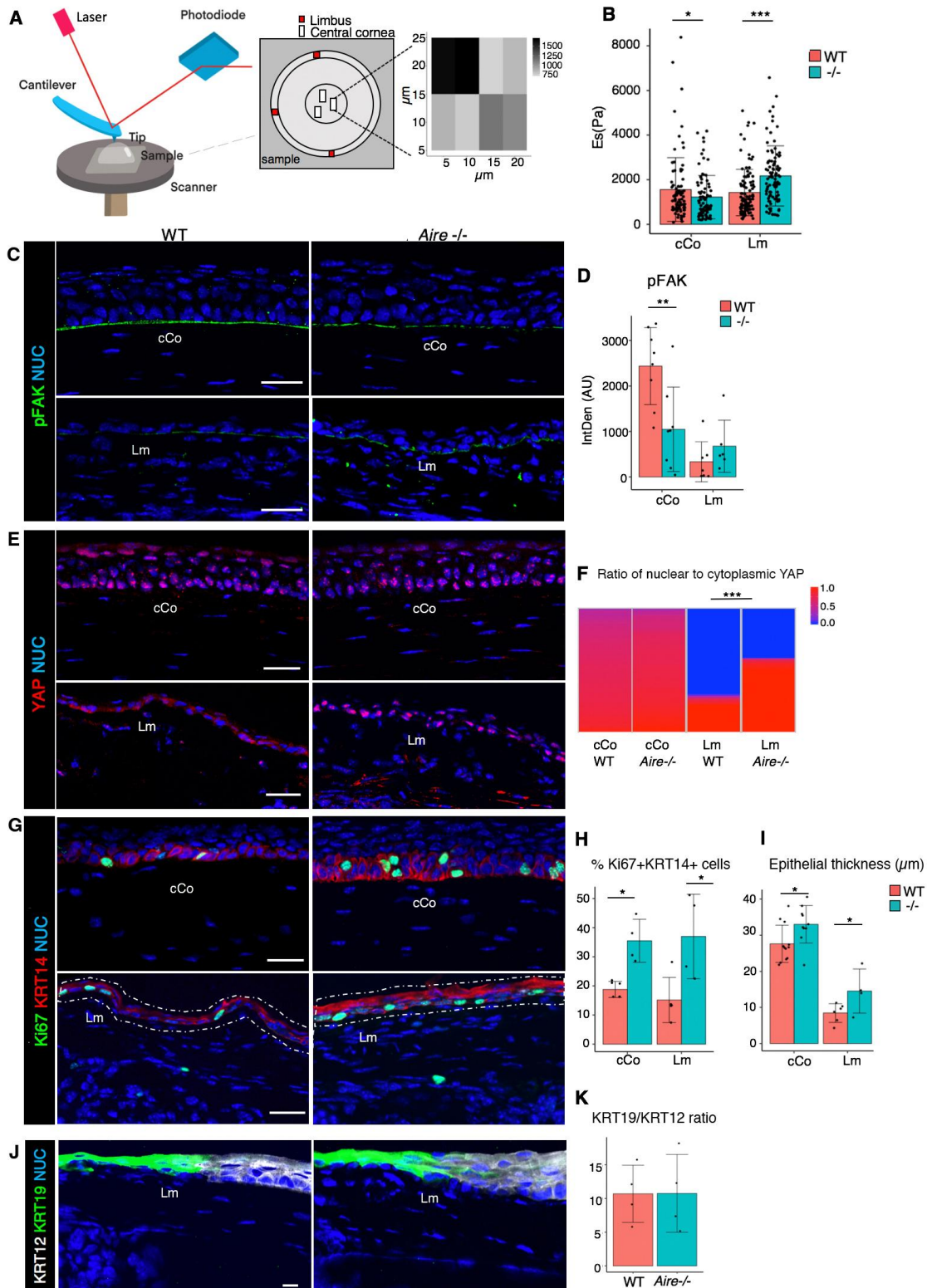


Figure 5



References:

- [1] S. Ienopoli, S.E. Carsons, Extraglandular manifestations of primary Sjögren's syndrome, *Oral Maxillofac. Surg. Clin. North Am.* (2014). <https://doi.org/10.1016/j.coms.2013.09.008>.
- [2] M.S. Sridhar, Anatomy of cornea and ocular surface, *Indian J. Ophthalmol.* (2018). https://doi.org/10.4103/ijo.IJO_646_17.
- [3] D.M. MAURICE, The structure and transparency of the cornea., *J. Physiol.* (1957). <https://doi.org/10.1113/jphysiol.1957.sp005758>.
- [4] H. Aubert, L. Mattieson, Graefe-Saemisch Handbuch der gesamten Augenheilkunde, Band I, Teil 2, Engelmann, Leipzig. (1876).
- [5] N. Di Girolamo, S. Bobba, V. Raviraj, N.C. Delic, I. Slapetova, P.R. Nicovich, G.M. Halliday, D. Wakefield, R. Whan, J.G. Lyons, Tracing the fate of limbal epithelial progenitor cells in the murine cornea, *Stem Cells.* (2015). <https://doi.org/10.1002/stem.1769>.
- [6] J.R. Mutch, The lacrimation reflex, *Br. J. Ophthalmol.* 28 (1944) 317.
- [7] A.P. del Palomar, A. Montolío, J. Cegoñino, S.K. Dhandra, C.T. Lio, T. Bose, The Innate Immune Cell Profile of the Cornea Predicts the Onset of Ocular Surface Inflammatory Disorders, *J. Clin. Med.* (2019). <https://doi.org/10.3390/jcm8122110>.
- [8] M.A. Lemp, C. Baudouin, J. Baum, M. Dogru, G.N. Foulks, S. Kinoshita, P. Laibson, J. McCulley, J. Murube, S.C. Pflugfelder, M. Rolando, I. Toda, The definition and classification of dry eye disease: Report of the definition and classification subcommittee of the international Dry Eye WorkShop (2007), in: *Ocul. Surf.*, 2007. [https://doi.org/10.1016/s1542-0124\(12\)70081-2](https://doi.org/10.1016/s1542-0124(12)70081-2).
- [9] S.C. Pflugfelder, S.C.G. Tseng, O. Sanabria, H. Kell, C.G. Garcia, C. Felix, W. Feuer, B.L. Reis, Evaluation of subjective assessments and objective diagnostic tests for diagnosing tear-film disorders known to cause ocular irritation, *Cornea.* (1998). <https://doi.org/10.1097/00003226-199801000-00007>.
- [10] F.Y. Chen, A. Lee, S. Ge, S. Nathan, S.M. Knox, N.A. McNamara, Aire-deficient mice provide a model of corneal and lacrimal gland neuropathy in Sjögren's syndrome, *PLoS One.* (2017). <https://doi.org/10.1371/journal.pone.0184916>.

- [11] K.S. Kunert, A.S. Tisdale, M.E. Stern, J.A. Smith, I.K. Gipson, Analysis of topical cyclosporine treatment of patients with dry eye syndrome: Effect on conjunctival lymphocytes, *Arch. Ophthalmol.* (2000). <https://doi.org/10.1001/archopht.118.11.1489>.
- [12] M.E. Stern, J. Gao, T.A. Schwalb, M. Ngo, D.D. Tieu, C.C. Chan, B.L. Reis, S.M. Whitcup, D. Thompson, J.A. Smith, Conjunctival T-cell subpopulations in Sjögren's and non-Sjögren's patients with dry eye, *Investig. Ophthalmol. Vis. Sci.* (2002).
- [13] D.A. Luce, Determining in vivo biomechanical properties of the cornea with an ocular response analyzer, *J. Cataract Refract. Surg.* (2005). <https://doi.org/10.1016/j.jcrs.2004.10.044>.
- [14] Q. Long, J.Y. Wang, D. Xu, Y. Li, Comparison of corneal biomechanics in Sjögren's syndrome and non-Sjögren's syndrome dry eyes by Scheimpflug based device, *Int. J. Ophthalmol.* (2017). <https://doi.org/10.18240/ijo.2017.05.08>.
- [15] H.B. Wallace, J. McKelvie, C.R. Green, S.L. Misra, Corneal curvature: The influence of corneal accommodation and biomechanics on corneal shape, *Transl. Vis. Sci. Technol.* (2019). <https://doi.org/10.1167/tvst.8.4.5>.
- [16] J. Ma, Y. Wang, P. Wei, V. Jhanji, Biomechanics and structure of the cornea: implications and association with corneal disorders, *Surv. Ophthalmol.* (2018). <https://doi.org/10.1016/j.survophthal.2018.05.004>.
- [17] K.M. Meek, R.H. Newton, Organization of collagen fibrils in the corneal stroma in relation to mechanical properties and surgical practice, *J. Refract. Surg.* (1999). <https://doi.org/10.3928/1081-597X-19991101-18>.
- [18] K.M. Meek, C. Boote, The organization of collagen in the corneal stroma, *Exp. Eye Res.* (2004). <https://doi.org/10.1016/j.exer.2003.07.003>.
- [19] G. Scarcelli, R. Pineda, S.H. Yun, Brillouin optical microscopy for corneal biomechanics, *Investig. Ophthalmol. Vis. Sci.* (2012). <https://doi.org/10.1167/iovs.11-8281>.
- [20] J. Hjortdal, Regional elastic performance of the human cornea, *J. Biomech.* (1996). [https://doi.org/10.1016/0021-9290\(95\)00152-2](https://doi.org/10.1016/0021-9290(95)00152-2).

- [21] T. Bongiorno, J.L. Chojnowski, J.D. Lauderdale, T. Sulchek, Cellular Stiffness as a Novel Stemness Marker in the Corneal Limbus, *Biophys. J.* (2016). <https://doi.org/10.1016/j.bpj.2016.09.005>.
- [22] J.J. DeVoss, A.K. Shum, K.P.A. Johannes, W. Lu, A.K. Krawisz, P. Wang, T. Yang, N.P. LeClair, C. Austin, E.C. Strauss, M.S. Anderson, Effector Mechanisms of the Autoimmune Syndrome in the Murine Model of Autoimmune Polyglandular Syndrome Type 1, *J. Immunol.* (2008). <https://doi.org/10.4049/jimmunol.181.6.4072>.
- [23] J.F. Meadows, K. Dionne, K.K. Nichols, Differential profiling of T-cell cytokines as measured by protein microarray across dry eye subgroups, *Cornea.* (2016). <https://doi.org/10.1097/ICO.0000000000000721>.
- [24] M.E.H. De Silva, L.J. Hill, L.E. Downie, H.R. Chinnery, The effects of aging on corneal and ocular surface homeostasis in mice, *Investig. Ophthalmol. Vis. Sci.* (2019). <https://doi.org/10.1167/iovs.19-26631>.
- [25] P. Xu, A. Londregan, C. Rich, V. Trinkaus-Randall, Changes in epithelial and stromal corneal stiffness occur with age and obesity, *Bioengineering.* (2020). <https://doi.org/10.3390/bioengineering7010014>.
- [26] C. Wang, T. Fu, C. Xia, Z. Li, Changes in mouse corneal epithelial innervation with age, *Investig. Ophthalmol. Vis. Sci.* (2012). <https://doi.org/10.1167/iovs.12-9704>.
- [27] F.Y.T. Chen, E. Gaylord, N. McNamara, S. Knox, Deciphering molecular and phenotypic changes associated with early autoimmune disease in the aire-deficient mouse model of Sjögren's syndrome, *Int. J. Mol. Sci.* (2018). <https://doi.org/10.3390/ijms19113628>.
- [28] W.-H. Tsai, Moment-preserving thresholding: A new approach, *Comput. Vision, Graph. Image Process.* 29 (1985) 377–393.
- [29] J.C. Yen, F.J. Chang, S. Chang, A New Criterion for Automatic Multilevel Thresholding, *IEEE Trans. Image Process.* (1995). <https://doi.org/10.1109/83.366472>.
- [30] S. Andrews, FastQC: a quality control tool for high throughput sequence data, (2010).

- [31] A. Dobin, C.A. Davis, F. Schlesinger, J. Drenkow, C. Zaleski, S. Jha, P. Batut, M. Chaisson, T.R. Gingeras, STAR: Ultrafast universal RNA-seq aligner, *Bioinformatics*. (2013). <https://doi.org/10.1093/bioinformatics/bts635>.
- [32] M.I. Love, W. Huber, S. Anders, Moderated estimation of fold change and dispersion for RNA-seq data with DESeq2, *Genome Biol.* (2014). <https://doi.org/10.1186/s13059-014-0550-8>.
- [33] K. Blighe, EnhancedVolcano: Publication-ready volcano plots with enhanced colouring and labeling. R package version 1.2. 0, (2019).
- [34] D.W. Huang, B.T. Sherman, R.A. Lempicki, Systematic and integrative analysis of large gene lists using DAVID bioinformatics resources, *Nat. Protoc.* (2009). <https://doi.org/10.1038/nprot.2008.211>.
- [35] A. Subramanian, P. Tamayo, V. Mootha, GSEA: Gene set enrichment analysis Gene set enrichment analysis: A knowledge-based approach for interpreting genome-wide expression profiles, *Pnsa*. (2014).
- [36] J.I. Lopez, I. Kang, W.K. You, D.M. McDonald, V.M. Weaver, In situ force mapping of mammary gland transformation, *Integr. Biol.* (2011). <https://doi.org/10.1039/c1ib00043h>.
- [37] Y.-S. Park, A. Gauna, S. Cha, Mouse Models of Primary Sjogren's Syndrome, *Curr. Pharm. Des.* (2015). <https://doi.org/10.2174/1381612821666150316120024>.
- [38] S. Filenius, M. Hormia, J. Rissanen, R.E. Burgeson, Y. Yamada, K. Araki-Sasaki, M. Nakamura, I. Virtanen, T. Tervo, Laminin synthesis and the adhesion characteristics of immortalized human corneal epithelial cells to laminin isoforms, *Exp. Eye Res.* (2001). <https://doi.org/10.1006/exer.2000.0933>.
- [39] J. Chlasta, P. Milani, G. Runel, J.L. Duteyrat, L. Arias, L.A. Lamiré, A. Boudaoud, M. Grammont, Variations in basement membrane mechanics are linked to epithelial morphogenesis, *Dev.* (2017). <https://doi.org/10.1242/dev.152652>.
- [40] C.S. Nowell, P.D. Odermatt, L. Azzolin, S. Hohnel, E.F. Wagner, G.E. Fantner, M.P. Lutolf, Y. Barrandon, S. Piccolo, F. Radtke, Chronic inflammation imposes aberrant cell fate in regenerating epithelia through mechanotransduction, *Nat. Cell Biol.* (2016). <https://doi.org/10.1038/ncb3290>.

- [41] Y. Qu, W. Chi, X. Hua, R. Deng, J. Li, Z. Liu, S.C. Pflugfelder, D.Q. Li, Unique expression pattern and functional role of periostin in human limbal stem cells, *PLoS One*. (2015). <https://doi.org/10.1371/journal.pone.0117139>.
- [42] T. Sakimoto, T. im Kim, D. Ellenberg, N. Fukai, S. Jain, D.T. Azar, J.H. Chang, Collagen XVIII and corneal reinnervation following keratectomy, *FEBS Lett*. (2008). <https://doi.org/10.1016/j.febslet.2008.09.052>.
- [43] G. Savini, The challenge of dry eye diagnosis, *Clin. Ophthalmol*. (2008). <https://doi.org/10.2147/ophth.s1496>.
- [44] F. Mantelli, J. Mauris, P. Argüeso, The ocular surface epithelial barrier and other mechanisms of mucosal protection: from allergy to infectious diseases, *Curr. Opin. Allergy Clin. Immunol*. (2013). <https://doi.org/10.1097/ACI.0b013e3283645899>.
- [45] M. Ristola, S. Lehtonen, Functions of the podocyte proteins nephrin and Neph3 and the transcriptional regulation of their genes, *Clin. Sci. (Lond)*. (2014). <https://doi.org/10.1042/CS20130258>.
- [46] J.F. Foley, EphA2 destabilizes adherens junctions, *Sci. Signal*. (2008). <https://doi.org/10.1126/stke.15ec47>.
- [47] R.H. Klein, W. Hu, G. Kashgari, Z. Lin, T. Nguyen, M. Doan, B. Andersen, Characterization of enhancers and the role of the transcription factor KLF7 in regulating corneal epithelial differentiation, *J. Biol. Chem*. (2017). <https://doi.org/10.1074/jbc.M117.793117>.
- [48] J.A. Segre, C. Bauer, E. Fuchs, Klf4 is a transcription factor required for establishing the barrier function of the skin, *Nat. Genet*. (1999). <https://doi.org/10.1038/11926>.
- [49] E.E. Delp, S. Swamynathan, W.W. Kao, S.K. Swamynathan, Spatiotemporally regulated ablation of Klf4 in adult mouse corneal epithelial cells results in altered epithelial cell identity and disrupted homeostasis, *Investig. Ophthalmol. Vis. Sci*. (2015). <https://doi.org/10.1167/iovs.15-16463>.
- [50] F. Van Roy, G. Berx, The cell-cell adhesion molecule E-cadherin, *Cell. Mol. Life Sci*. (2008). <https://doi.org/10.1007/s00018-008-8281-1>.
- [51] A.S. Fanning, J.M. Anderson, Zonula occludens-1 and-2 are cytosolic scaffolds that regulate the assembly of cellular junctions, *Ann. N. Y. Acad. Sci*. 1165 (2009) 113.

- [52] S.P. Sugrue, J.D. Zieske, ZO1 in corneal epithelium: Association to the zonula occludens and adherens junctions, *Exp. Eye Res.* (1997). <https://doi.org/10.1006/exer.1996.0175>.
- [53] M.A. Stepp, H.E. Gibson, P.H. Gala, D.D. Drina, A. Pajooohesh-Ganji, S. Pal-Ghosh, M. Brown, C. Aquino, A.M. Schwartz, O. Goldberger, M.T. Hinkes, M. Bernfield, Defects in keratinocyte activation during wound healing in the syndecan-1-deficient mouse, *J. Cell Sci.* (2002). <https://doi.org/10.1242/jcs.00128>.
- [54] W.P. Daley, S.B. Peters, M. Larsen, Extracellular matrix dynamics in development and regenerative medicine, *J. Cell Sci.* (2008). <https://doi.org/10.1242/jcs.006064>.
- [55] T.R. Cox, J.T. Eler, Remodeling and homeostasis of the extracellular matrix: Implications for fibrotic diseases and cancer, *DMM Dis. Model. Mech.* (2011). <https://doi.org/10.1242/dmm.004077>.
- [56] J.D. Humphrey, E.R. Dufresne, M.A. Schwartz, Mechanotransduction and extracellular matrix homeostasis, *Nat. Rev. Mol. Cell Biol.* (2014). <https://doi.org/10.1038/nrm3896>.
- [57] R.M. Gouveia, G. Lepert, S. Gupta, R.R. Mohan, C. Paterson, C.J. Connon, Assessment of corneal substrate biomechanics and its effect on epithelial stem cell maintenance and differentiation, *Nat. Commun.* (2019). <https://doi.org/10.1038/s41467-019-09331-6>.
- [58] P. Tomakidi, S. Schulz, S. Proksch, W. Weber, T. Steinberg, Focal adhesion kinase (FAK) perspectives in mechanobiology: implications for cell behaviour, *Cell Tissue Res.* (2014). <https://doi.org/10.1007/s00441-014-1945-2>.
- [59] D. Lachowski, E. Cortes, B. Robinson, A. Rice, K. Rombouts, A.E. Del Río Hernández, FAK controls the mechanical activation of YAP, a transcriptional regulator required for durotaxis, *FASEB J.* (2018). <https://doi.org/10.1096/fj.201700721R>.
- [60] O. Dobrokhotov, M. Samsonov, M. Sokabe, H. Hirata, Mechanoregulation and pathology of YAP/TAZ via Hippo and non-Hippo mechanisms, *Clin. Transl. Med.* 7 (2018) 1–14.
- [61] S. Masterton, M. Ahearne, Mechanobiology of the corneal epithelium, *Exp. Eye Res.* (2018). <https://doi.org/10.1016/j.exer.2018.08.001>.

- [62] Y.T. Chen, F.Y.T. Chen, T. Vijmasi, D.N. Stephens, M. Gallup, N.A. McNamara, Pax6 Downregulation Mediates Abnormal Lineage Commitment of the Ocular Surface Epithelium in Aqueous-Deficient Dry Eye Disease, *PLoS One*. (2013). <https://doi.org/10.1371/journal.pone.0077286>.
- [63] S. Kling, F. Hafezi, Corneal biomechanics – a review, *Ophthalmic Physiol. Opt.* (2017). <https://doi.org/10.1111/opo.12345>.
- [64] R.G. Wells, The role of matrix stiffness in regulating cell behavior, *Hepatology*. (2008). <https://doi.org/10.1002/hep.22193>.
- [65] J.A. Last, S.M. Thomasy, C.R. Croasdale, P. Russell, C.J. Murphy, Compliance profile of the human cornea as measured by atomic force microscopy, *Micron*. (2012). <https://doi.org/10.1016/j.micron.2012.02.014>.
- [66] M. Winkler, D. Chai, S. Kriling, C.J. Nien, D.J. Brown, B. Jester, T. Juhasz, J. V. Jester, Nonlinear optical macroscopic assessment of 3-D corneal collagen organization and axial biomechanics, *Investig. Ophthalmol. Vis. Sci.* (2011). <https://doi.org/10.1167/iovs.11-8070>.
- [67] R.R. Jones, I.W. Hamley, C.J. Connon, Ex vivo expansion of limbal stem cells is affected by substrate properties, *Stem Cell Res.* (2012). <https://doi.org/10.1016/j.scr.2012.01.001>.
- [68] J.W. Foster, R.R. Jones, C.A. Bippes, R.M. Gouveia, C.J. Connon, Differential nuclear expression of Yap in basal epithelial cells across the cornea and substrates of differing stiffness, *Exp. Eye Res.* (2014). <https://doi.org/10.1016/j.exer.2014.06.020>.
- [69] P. Eberwein, T. Reinhard, Concise reviews: The role of biomechanics in the limbal stem cell niche: New insights for our understanding of this structure, *Stem Cells*. (2015). <https://doi.org/10.1002/stem.1886>.
- [70] K. Taniguchi, L.W. Wu, S.I. Grivennikov, P.R. De Jong, I. Lian, F.X. Yu, K. Wang, S.B. Ho, B.S. Boland, J.T. Chang, W.J. Sandborn, G. Hardiman, E. Raz, Y. Maehara, A. Yoshimura, J. Zucman-Rossi, K.L. Guan, M. Karin, A gp130-Src-YAP module links inflammation to epithelial regeneration, *Nature*. (2015). <https://doi.org/10.1038/nature14228>.

- [71] A.A.M. Torricelli, V. Singh, M.R. Santhiago, S.E. Wilson, The corneal epithelial basement membrane: Structure, function, and disease, *Investig. Ophthalmol. Vis. Sci.* (2013). <https://doi.org/10.1167/iovs.13-12547>.
- [72] S.E. Wilson, L. Chen, R.R. Mohan, Q. Liang, L. Janice, Expression of HGF, KGF, EGF and receptor messenger RNAs following corneal epithelial wounding, *Exp. Eye Res.* (1999). <https://doi.org/10.1006/exer.1998.0603>.
- [73] L. Zhang, M.C. Anderson, C.-Y. Liu, The role of corneal stroma: A potential nutritional source for the cornea., *J. Nat. Sci.* (2017).
- [74] K. Brejchova, P. Liskova, E. Hrdlickova, M. Filipec, K. Jirsova, Matrix metalloproteinases in recurrent corneal melting associated with primary Sjögren's syndrome., *Mol. Vis.* (2009).
- [75] J.S. Weiss, H.U. Møller, A.J. Aldave, B. Seitz, C. Bredrup, T. Kivelä, F.L. Munier, C.J. Rapuano, K.K. Nischal, E.K. Kim, J. Sutphin, M. Busin, A. Labbé, K.R. Kenyon, S. Kinoshita, W. Lisch, IC3D classification of corneal dystrophies-edition 2, *Cornea.* (2015). <https://doi.org/10.1097/ICO.0000000000000307>.
- [76] D.T. Azar, S.J. Spurr Michaud, A.S. Tisdale, I.K. Gipson, Altered Epithelial-Basement Membrane Interactions in Diabetic Corneas, *Arch. Ophthalmol.* (1992). <https://doi.org/10.1001/archopht.1992.01080160115045>.
- [77] R.M. Corrales, M.E. Stern, C.S. De Paiva, J. Welch, D.Q. Li, S.C. Pflugfelder, Desiccating stress stimulates expression of matrix metalloproteinases by the corneal epithelium, *Investig. Ophthalmol. Vis. Sci.* (2006). <https://doi.org/10.1167/iovs.05-1382>.
- [78] D.Q. Li, Z. Chen, X.J. Song, L. Luo, S.C. Pflugfelder, Stimulation of matrix metalloproteinases by hyperosmolarity via a JNK pathway in human corneal epithelial cells, *Investig. Ophthalmol. Vis. Sci.* (2004). <https://doi.org/10.1167/iovs.04-0299>.
- [79] N.D. Rawlings, M. Waller, A.J. Barrett, A. Bateman, MEROPS: The database of proteolytic enzymes, their substrates and inhibitors, *Nucleic Acids Res.* (2014). <https://doi.org/10.1093/nar/gkt953>.

- [80] S. Pal-Ghosh, T. Blanco, G. Tadvalkar, A. Pajoohesh-Ganji, A. Parthasarathy, J.D. Zieske, M.A. Stepp, MMP9 cleavage of the β 4 integrin ectodomain leads to recurrent epithelial erosions in mice, *J. Cell Sci.* (2011). <https://doi.org/10.1242/jcs.085480>.
- [81] J.M. Whitelock, A.D. Murdoch, R. V. Iozzo, P.A. Underwood, The degradation of human endothelial cell-derived perlecan and release of bound basic fibroblast growth factor by stromelysin, collagenase, plasmin, and heparanases, *J. Biol. Chem.* (1996). <https://doi.org/10.1074/jbc.271.17.10079>.
- [82] L. Sobrin, Z. Liu, D.C. Monroy, A. Solomon, M.G. Selzer, B.L. Lokeshwar, S.C. Pflugfelder, Regulation of MMP-9 activity in human tear fluid and corneal epithelial culture supernatant, *Investig. Ophthalmol. Vis. Sci.* (2000).
- [83] M.T. Kuo, P.C. Fang, T.L. Chao, A. Chen, Y.H. Lai, Y.T. Huang, C.Y. Tseng, Tear proteomics approach to monitoring Sjögren syndrome or dry eye disease, *Int. J. Mol. Sci.* (2019). <https://doi.org/10.3390/ijms20081932>.
- [84] Y. Xia, S. Lian, P.N. Khoi, H.J. Yoon, Y.E. Joo, K.O. Chay, K.K. Kim, Y. Do Jung, Chrysin inhibits tumor promoter-induced MMP-9 expression by blocking AP-1 via suppression of ERK and JNK pathways in gastric cancer cells, *PLoS One.* 10 (2015).
- [85] H.C. Tseng, I.T. Lee, C.C. Lin, P.L. Chi, S.E. Cheng, R.H. Shih, L. Der Hsiao, C.M. Yang, IL-1 β Promotes Corneal Epithelial Cell Migration by Increasing MMP-9 Expression through NF- κ B- and AP-1-Dependent Pathways, *PLoS One.* (2013). <https://doi.org/10.1371/journal.pone.0057955>.
- [86] C.-Y. Cheng, H.-L. Hsieh, L.-D. Hsiao, C.-M. Yang, PI3-K/Akt/JNK/NF- κ B is essential for MMP-9 expression and outgrowth in human limbal epithelial cells on intact amniotic membrane, *Stem Cell Res.* 9 (2012) 9–23.
- [87] F. Legendre, P. Bogdanowicz, K. Boumediene, J.-P. Pujol, Role of interleukin 6 (IL-6)/IL-6R-induced signal transducers and activators of transcription and mitogen-activated protein kinase/extracellular., *J. Rheumatol.* 32 (2005) 1307–1316.
- [88] H.K. Koul, M. Pal, S. Koul, Role of p38 MAP Kinase Signal Transduction in Solid Tumors, *Genes and Cancer.* (2013). <https://doi.org/10.1177/1947601913507951>.
- [89] A. Basu, J.K. Krady, S.W. Levison, Interleukin-1: A master regulator of neuroinflammation, *J. Neurosci. Res.* (2004). <https://doi.org/10.1002/jnr.20266>.

- [90] R. Ambrósio, F. Faria-Correia, I. Ramos, B.F. Valbon, B. Lopes, D. Jardim, A. Luz, Enhanced Screening for Ectasia Susceptibility Among Refractive Candidates: The Role of Corneal Tomography and Biomechanics, *Curr. Ophthalmol. Rep.* (2013). <https://doi.org/10.1007/s40135-012-0003-z>.
- [91] S. Kaushik, S.S. Pandav, Ocular response analyzer, *J. Curr. Glaucoma Pract.* (2012). <https://doi.org/10.5005/jp-journals-10008-1103>.
- [92] C.W. Mcmonnies, The potential role of neuropathic mechanisms in dry eye syndromes, *J. Optom.* (2017). <https://doi.org/10.1016/j.optom.2016.06.002>.
- [93] A.C. de Luca, S.P. Lacour, W. Raffoul, P.G. di Summa, Extracellular matrix components in peripheral nerve repair: How to affect neural cellular response and nerve regeneration?, *Neural Regen. Res.* (2014). <https://doi.org/10.4103/1673-5374.145366>.
- [94] A.D. Lander, D.K. Fujii, L.F. Reichardt, Purification of a factor that promotes neurite outgrowth: Isolation of laminin and associated molecules, *J. Cell Biol.* (1985). <https://doi.org/10.1083/jcb.101.3.898>.
- [95] P.S.-Y. Lee, N. Gao, M. Dike, O. Shkilnyy, R. Me, Y. Zhang, X.Y. Fu-Shin, Opposing Effects of Neuropilin-1 and-2 on Sensory Nerve Regeneration in Wounded Corneas: Role of Sema3C in Ameliorating Diabetic Neurotrophic Keratopathy, *Diabetes*. 68 (2019) 807–818.
- [96] P. Demetter, M. De Vos, N. Van Damme, D. Baeten, D. Elewaut, S. Vermeulen, M. Mareel, G. Bullock, H. Mielants, G. Verbruggen, F. De Keyser, E.M. Veys, C.A. Cuvelier, Focal up-regulation of E-cadherin-catenin complex in inflamed bowel mucosa but reduced expression in ulcer-associated cell lineage, *Am. J. Clin. Pathol.* (2000). <https://doi.org/10.1093/ajcp/114.3.364>.
- [97] A.W. Stadnyk, Cytokine production by epithelial cells., *FASEB J.* (1994). <https://doi.org/10.1096/fasebj.8.13.7926369>.
- [98] R.M. Al-Sadi, T.Y. Ma, IL-1 β Causes an Increase in Intestinal Epithelial Tight Junction Permeability, *J. Immunol.* (2007). <https://doi.org/10.4049/jimmunol.178.7.4641>.

- [99] T. Abe, E. Sugano, Y. Saigo, M. Tamai, Interleukin-1 β and barrier function of retinal pigment epithelial cells (ARPE-19): aberrant expression of junctional complex molecules, *Invest. Ophthalmol. Vis. Sci.* 44 (2003) 4097–4104.
- [100] K. Kimura, S. Teranishi, T. Nishida, Interleukin-1 β -induced disruption of barrier function in cultured human corneal epithelial cells, *Investig. Ophthalmol. Vis. Sci.* (2009). <https://doi.org/10.1167/iovs.08-2606>.
- [101] Y.T. Chen, S. Lazarev, A.F. Bahrami, L.B. Noble, F.Y.T. Chen, D. Zhou, M. Gallup, M. Yadav, N.A. McNamara, Interleukin-1 receptor mediates the interplay between CD4 + T cells and ocular resident cells to promote keratinizing squamous metaplasia in Sjögren's syndrome, *Lab. Invest.* (2012). <https://doi.org/10.1038/labinvest.2011.189>.
- [102] A. Bukowiecki, D. Hos, C. Cursiefen, S.A. Eming, Wound-healing studies in cornea and skin: Parallels, differences and opportunities, *Int. J. Mol. Sci.* (2017). <https://doi.org/10.3390/ijms18061257>.